

Influence of quantum critical point of first order valence transition on Ce- and Yb-based heavy fermions

Shinji Watanabe^{*1}, Kazumasa Miyake²

¹ Department of Applied Physics, University of Tokyo, Hongo 7-3-1, Bunkyo-ku, Tokyo, 113-8656, Japan^{**}

² Division of Materials Physics, Department of Materials Engineering Science, Graduate School of Engineering Science, Osaka University, Toyonaka, Osaka 560-8531, Japan

Received 10 June 2009, revised 14 January 2010, accepted 14 January 2010

Published online online 17 February 2010

PACS 71.10.-w, 71.20.Eh, 71.27.+a, 74.70.Tx, 75.40.-s

* Corresponding author: **Present address: Division of Materials Physics, Department of Materials Engineering Science, Graduate School of Engineering Science, Osaka University, Toyonaka, Osaka 560-8531, Japan

Influence of quantum critical point (QCP) of first-order valence transition (FOVT) on Ce- and Yb-based heavy fermions is discussed as a key origin of anomalies such as non-Fermi liquid, metamagnetism, and unconventional superconductivity. Even in intermediate-valence materials, the QCP of the FOVT is shown to be induced by applying the magnetic field, which creates a new characteristic energy distinct from the Kondo temperature.

It is stressed that the key concept is closeness to the QCP of the FOVT by pointing out that the proximity of the QCP explains sharp contrast between X=Ag and X=Cd in YbXCu₄, field-induced valence crossover in X=Au, and field-induced first order transition as well as non-Fermi-liquid critical behaviours in CeIrIn₅. The valence fluctuations can be a key origin of unresolved phenomena in this family of materials.

Copyright line will be provided by the publisher

1 Introduction Quantum critical phenomena in itinerant fermion systems have been intensively studied in the context of spin fluctuations [1-3]. Recently, quantum critical phenomena in charge degrees of freedom have attracted much attention [4]. One of such highlights is valence transition, which is a phase transition with a valence of materials element showing a discontinuous jump. A typical example is known as the γ - α transition in Ce metal, where the isostructural first-order valence transition (FOVT) occurs in temperature-pressure (T, P) phase diagram [5] (see Fig. 1(a)). The valence of Ce changes discontinuously between Ce^{+3.03} (γ phase) and Ce^{+3.14} (α phase) at $T = 300$ K [6]. The FOVT line terminates at the critical end point at $(T, P) = (600 \text{ K}, 2 \text{ GPa})$. As diverging density fluctuations at the critical end point in the liquid-gas transition, valence fluctuations diverge at the critical end point. In Ce metal, the critical-end temperature is so high that quantum criticality has not been discovered.

When the critical-end temperature is suppressed to $T = 0 \text{ K}$ by changing materials parameters, the quantum critical end point emerges. Since the quantum crit-

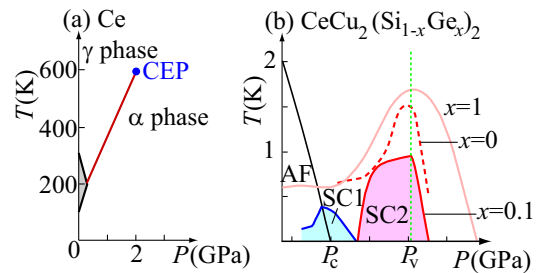


Figure 1 (color online) T - P phase diagram of (a) Ce and (b) $\text{CeCu}_2(\text{Si}_{1-x}\text{Ge}_x)_2$. (a) FOVT between the γ and α phases terminates at the critical end point (CEP). (b) Unified phase diagram of $x = 0$ [8], $x = 0.1$ [10], and $x = 1$ [7]. As for P axis, $P_v = 4.5 \text{ GPa}$ ($x = 0$), $P_v = 5.5 \text{ GPa}$ ($x = 0.1$), and $P_v = 15.5 \text{ GPa}$ ($x = 1$) are set as the same position (see ref. [10] for details). The dotted line at P_v is a guide for the eyes.

Copyright line will be provided by the publisher

ical point (QCP) is defined as the point at which the continuous-transition temperature touches $T = 0$ K, we refer to the quantum critical end point as the QCP in this paper. The quantum criticality and electron instabilities arisen from the QCP of the FOVT has been recognized as emergence of two superconducting domes in the T - P phase diagram of CeCu_2Ge_2 [7], CeCu_2Si_2 [8,9], and $\text{CeCu}_2(\text{Si}_x\text{Ge}_{1-x})_2$ [10,11]: Near the QCP $P = P_c$ where the Neel temperature is suppressed under pressure, a superconducting phase emerges (SC1). Interestingly, further enhancement of the superconducting-transition temperature T_{SC} emerges by further applying pressure (SC2) (see Fig. 1(b)). Around the pressure $P = P_v$ where T_{SC} has a maximum in the SC2, the quantum critical behaviours such as a T -linear resistivity and a remarkable enhancement of residual resistivity have been observed. Since the resistivity shows the $T^{1.5}$ dependence near $P = P_c$, i.e., the criticality predicted theoretically for the antiferromagnetic (AF) QCP in three spatial dimension [1-3], these anomalies near $P = P_v$ should be ascribed to a distinct origin of AF quantum criticality.

Theoretically, a possibility of emergence of valence criticality at $P = P_v$ has been pointed out in ref. [12]: A key experimental feature is the pressure dependence of the T^2 coefficient A estimated from the low-temperature part of resistivity [4]. A remarkable fact is that A sharply decreases with 2-3 orders of magnitude, when P increases and across $P = P_v$ [7-11]. Since A is proportional to γ_e^2 with γ_e being Sommerfeld constant by so-called Kadowaki-Woods relation [13], this suggests that the effective mass of electrons m^*/m_0 is drastically reduced at $P = P_v$. This sharp crossover is also reflected in the sharp change of the Kadowaki-Woods ratio between strong-correlation regime $A/\gamma_e^2 = 10^{-5}$ ($P < P_v$) and weak-correlation regime $A/\gamma_e^2 = 10^{-6}$ ($P > P_v$). If we remind the fact that the effective mass is expressed by the f -electron number per site in Ce (and also Yb for the f -hole number) based heavy fermion systems: $m^*/m_0 \propto (1 - n_f/2)/(1 - n_f)$ shown by the Gutzwiller arguments for periodic Anderson model [14], the above observations imply that the f -electron number is sharply deviated from $n_f \sim 1$ when P exceeds P_v . In other words, the valence of Ce increases sharply from nearly trivalent $3+$ ($n_f \sim 1$) realized in the low-pressure regime to a larger valence $3 + \delta$ ($n_f \sim 1 - \delta$) with δ being a positive value.

Recent ^{63}Cu NQR measurement in CeCu_2Si_2 under pressure has detected that near $P = P_v \sim 4.5$ GPa the NQR frequency ν_Q starts to deviate from linear increase expected from the monotonic volume shrinkage under hydrostatic pressure [9]. The downward deviation from the monotonic increase in the ν_Q - P plane indicates that the charge distribution around the Cu site changes around $P = P_v$, strongly suggesting that the Ce valence changes at $P = P_v$. Enhanced valence fluctuations have been shown theoretically to make the impurity scattering strong, giving rise to the enhancement of the residual resistivity [15]. The

local nature of valence fluctuations has been also shown to cause the non-Fermi-liquid critical behaviour in the resistivity: The T -linear dependence emerges near the QCP of the FOVT [8].

In Fig. 1(b), T_{SC} in the SC2 starts to increase at the lower pressure than P_v , i.e., just before the Ce valence increases. After the sharp valence crossover for $P > P_v$, the superconductivity is immediately suppressed. This feature is reproduced by the slave-boson mean-field theory taking into account of Gaussian fluctuations applied to the periodic Anderson model with an inter-orbital Coulomb repulsion (see Eq. (1) below) [16]: In the lower pressure region than P_v , T_{SC} is enhanced. The density matrix renormalization group (DMRG) calculation in the same model in one spatial dimension also shows that the enhancement of the superconducting correlation occurs for $P < P_v$ near the QCP [17]. It is noted that the valence-fluctuation mediated pairing mechanism proposed in ref. [12] obtained the firm grounds by unbiased numerical calculation [17].

Yb systems provide a hole analog of Ce systems, where in the $4f$ shell Yb^{3+} gives 13 electrons and Yb^{2+} gives fully occupied 14 electrons. Thus, in the hole picture $n_f = 1$ ($n_f = 0$) is realized for Yb^{3+} (Yb^{2+}). In Yb systems, the isostructural FOVT has been also known to occur in YbInCu_4 [18,19]: As T decreases, the first-order transition from $\text{Yb}^{+2.97}$ ($n_f = 0.97$) to $\text{Yb}^{+2.84}$ ($n_f = 0.84$) takes place at $T = 42$ K [20]. In the series of YbXCu_4 , when $X=\text{In}$ is replaced to the other elements such as $X=\text{Ag}$ [19,21] and Au [22], the first-order transition has not been observed. However, anomalous behaviours such as metamagnetism [19] and emergence of new characteristic energy scale distinct from the Kondo temperature [19,22] have been observed, which seem to be related to the enhanced valence fluctuations.

The critical behaviours and electronic instabilities observed in the Ce- and Yb-based systems seem to indicate a strong influence of the QCP of the valence transition. As seen in Fig. 1(a), the FOVT terminates at the critical end point in the T - P phase diagram in Ce metal. When the critical-end temperature is suppressed by controlling materials parameters, and enters into the Fermi degeneracy regime, the diverging valence fluctuations are considered to be coupled to the Fermi-surface instability. This combined effect of critical fluctuations and quantum fluctuations seems to be a key mechanism in understanding the anomalous Ce- and Yb-based heavy fermions. In the following sections, we show how the QCP of valence transition is controlled by the magnetic field, and discuss its influence on Ce- and Yb-based systems in the subsequent section.

2 Field-induced QCP of valence transition We analyze the magnetic field dependence of the QCP of the FOVT on the basis of the extended periodic Anderson model as a simplest minimal model for Ce- and Yb-based

heavy fermions:

$$H = H_c + H_f + H_{\text{hyb}} + H_{U_{fc}} - h \sum_i (S_i^{fz} + S_i^{cz}) \quad (1)$$

where $H_c = \sum_{\mathbf{k}\sigma} c_{\mathbf{k}\sigma}^\dagger c_{\mathbf{k}\sigma}$, $H_f = \sum_{i\sigma} f_{i\sigma}^\dagger f_{i\sigma} + U \sum_i f_{i\uparrow}^\dagger f_{i\uparrow} f_{i\downarrow}^\dagger f_{i\downarrow}$, $H_{\text{hyb}} = \sum_{i\sigma} (f_{i\sigma}^\dagger c_{i\sigma} + c_{i\sigma}^\dagger f_{i\sigma})$, and $H_{U_{fc}} = U_{fc} \sum_{i\sigma\sigma'} f_{i\sigma}^\dagger f_{i\sigma} c_{i\sigma'}^\dagger c_{i\sigma'}$. The U_{fc} term is the Coulomb repulsion between f and conduction electrons, and is considered to play an important role in the valence transition. For example, in the case of Ce metal which exhibits the γ - α transition, the $4f$ - and $5d$ -electron bands are located at the Fermi level [23]. Since both the orbitals are located on the same Ce site, this term cannot be neglected. In the case of YbInCu₄, $H_{U_{fc}}$ also plays a crucial role for the FOVT in the hole picture of Eq. (1) [24]. Most of Ce- and Yb-based compounds seem to have moderate values of U_{fc} . However, they seem to be affected by close proximity to the QCP of the FOVT as discussed below, which requires a moderate magnitude of U_{fc} in Eq. (1).

By applying the slave-boson mean-field theory [16] to Eq. (1), we have determined the locus of QCP of the FOVT under the magnetic field [25]. Figure 2 shows the ground-state phase diagram in the ε_f - U_{fc} plane for $D = 1$, $V = 0.5$, and $U = \infty$ at $n = (n_f + n_c)/2 = 7/8$, where the conduction band is set as $\varepsilon_{\mathbf{k}} = k^2/(2m) - D$ in three spatial dimension, and n_c is a conduction-electron number per site. At $h = 0$, when ε_f is deep enough, the Kondo state with $n_f = 1$ is realized. When ε_f approaches the Fermi level, f electrons are moved into the conduction band via hybridization, giving rise to the mixed-valence state with $n_f < 1$. The FOVT between them is caused by U_{fc} , since large U_{fc} forces electrons to pour from the f level into the conduction band. The FOVT line (solid line with open triangles) terminates at the QCP (filled circle), where the valence susceptibility $\chi_v \equiv -\partial n_f / \partial \varepsilon_f$, i.e., valence fluctuation, diverges. The dashed line represents the points where χ_v has a maximum as a function of ε_f for each U_{fc} , implying that even in the valence-crossover regime valence fluctuations are well developed. Note that the hybridization between f and conduction electrons is always finite in the ε_f - U_{fc} plane shown in Fig. 2. Hence, the Fermi surface is always large [17].

Under the magnetic field, the QCP shows non-monotonic field dependence as shown in Fig. 2: The QCP shifts to the smaller- U_{fc} and larger- ε_f direction for small h , and upturn behaviour emerges for $h \geq 0.04$. Since the Kondo temperature at the QCP $(\varepsilon_f^{\text{QCP}}, U_{fc}^{\text{QCP}}) = (0.356, 1.464)$ under $h = 0$ is estimated as $T_K^{\text{QCP}} = 0.074$, the characteristic field of the beginning of the upturn roughly corresponds to T_K^{QCP} . The origin of the upturn is due to the broadening of the spectral weight of f - and conduction-electrons Green function by the magnetic field larger than T_K^{QCP} [25]. If Ce- and Yb-based materials are located just on the locus of QCP's for $h > 0$ (a gray line) in Fig. 2, the metamagnetism will be observed at $h = h_m$

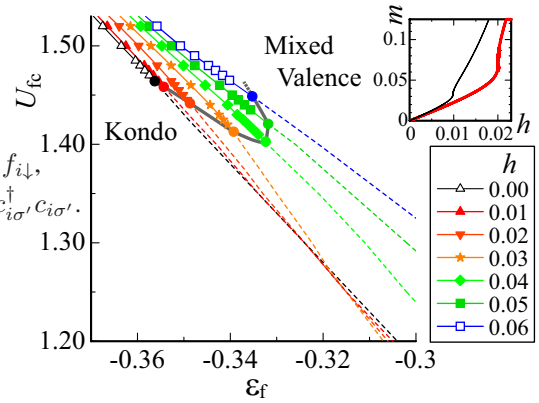


Figure 2 (color online) Ground-state phase diagram in the ε_f - U_{fc} plane for $D = 1$, $V = 0.5$, and $U = \infty$ at $n = 7/8$. The FOVT line with a QCP for $h = 0.00$ (open triangle), $h = 0.01$ (filled triangle), $h = 0.02$ (filled inverse triangle), $h = 0.03$ (filled star), $h = 0.04$ (filled diamond), $h = 0.05$ (filled square) and $h = 0.06$ (open square). The gray line connects the QCP's under h , which is a guide for the eyes. The dashed lines represent the valence-crossover points at which χ_v has a maximum as a function of ε_f for each U_{fc} . Inset: m - h curve for $(\varepsilon_f, U_{fc}) = (-0.354, 1.458)$ (thin line) and $(-0.349, 1.442)$ (bold line). m is defined by $m \equiv \sum_i (\langle S_i^{fz} \rangle + \langle S_i^{cz} \rangle) / N$.

(as seen in inset of Fig. 2). It is remarked that at the field-induced valence QCP, not only valence susceptibility χ_v , but also the magnetic susceptibility $\chi_s \equiv -\partial m / \partial h$ diverges. Thus, uniform spin fluctuations at $k = 0$ are also enhanced.

It is noted that the field-induced QCP of the FOVT has also been confirmed by the DMRG calculation in Eq. (1) in one dimension [25]. This indicates that not only unbiased calculation reproduces the above result, but also a difference of spatial dimensions does not alter the main conclusion. This is ascribed to the locality of the valence transition, which has a local atomic origin [26].

The metamagnetic field $h = h_m$ corresponds to the difference of T_K at the QCP between $h = 0$ and $h = h_m$: $h_m \sim T_K^{\text{QCP}}(h \neq 0) - T_K^{\text{QCP}}(h = 0)$. This indicates that there appears a distinct energy scale from the Kondo temperature, which is characterized by the closeness to the QCP of the FOVT. As mentioned above, Ce metal is considered to have a considerable value of U_{fc} due to its onsite origin. Hence, it seems to be located at $U_{fc} > U_{fc}^{\text{QCP}}$ in Fig. 2, giving rise to the FOVT. On the other hand, in Ce-based compounds, the energy bands located at the Fermi level usually consist of $4f$ orbitals at the Ce site and non- $4f$ orbitals at the non-Ce site. For example, $4f$ orbitals at the Ce site and $3p$ ($4p$) orbitals at the X site are responsible for the bands in CeCu₂X₂ (X=Si (Ge)). Then, U_{fc} has the intersite origin in Ce compounds. Hence, most of Ce- and also Yb-based compounds are considered to be

located in the intermediate valence-crossover regime for $U_{fc} < U_{fc}^{\text{QCP}}$ in Fig. 2. This is consistent with the experimental fact that most of those compounds do not show the FOVT, but merely show the valence crossover. However, the results revealed in Fig. 2 indicate that even such compounds can be affected by the proximity to the valence QCP by applying the magnetic field. In the next section, we discuss how this newly clarified mechanism resolves the outstanding puzzles measured in Ce- and Yb-based compounds so far.

3 Comparison with experiments

3.1 YbAgCu₄ and YbCdCu₄ YbAgCu₄ and YbCdCu₄ have paramagnetic-metal ground states. The analysis of T dependence of uniform magnetic susceptibilities of YbAgCu₄ and YbCdCu₄ concluded that both have nearly the same Kondo temperatures, about 200 K [19]. However, only in YbAgCu₄ a peak structure appears in the magnetic susceptibility around $T \sim 40$ K, but in YbCdCu₄ a conventional Pauli paramagnetism appears [19]. Such a contrast has been also detected in the magnetic-field response: YbAgCu₄ shows a metamagnetic increase of the magnetization around $h \sim 40$ T, while YbCdCu₄ does not [19]. These observations suggest that there exist a distinct energy scale from the Kondo temperature.

Our results explain this sharp contrast. Figure 3(a) shows the schematic contour plot of the f -hole number per site, n_f , which can be also regarded as the contour plot of the Kondo temperature, $T_K \propto (1 - n_f)/(1 - n_f/2)$ [14]. In the small (large) ε_f and U_{fc} regime, the Kondo (mixed valence) state with $n_f = 1$ ($n_f < 1$), i.e., small (large) T_K is realized. Since YbAgCu₄ and YbCdCu₄ have nearly the same T_K , both are considered to be located in the same contour area (see Fig. 3). If YbAgCu₄ is closer to the QCP with a distance about $h \sim 40$ T than YbCdCu₄ which is less close to the QCP, the metamagnetic behaviour in YbAgCu₄ at $h \sim 40$ T can be naturally understood.

This picture also gives a natural explanation for the origin of the peak structure observed in the uniform susceptibility at $T \sim 40$ K in YbAgCu₄. Figure 3(b) illustrates a schematic phase diagram of the T - ε_f - U_{fc} space. As shown in inset of Fig. 2, the metamagnetism with diverging magnetic susceptibility emerges at the QCP as well as the critical end points represented by the thick solid line with a circle in Fig. 3(b). An important result is that even at the valence-crossover surface extended from the FOVT surface in Fig. 3(b), the magnetic susceptibility χ_s as well as the valence susceptibility χ_v is enhanced [26]. If YbAgCu₄ touches the valence-crossover surface at about $T_v^* \sim 40$ K, the observed peak in $\chi_s(T)$ at $T \sim 40$ K is naturally explained. The reason of no conspicuous peak in $\chi_s(T)$ in YbCdCu₄ can be understood as too large temperature interval to touch the valence-crossover surface (see Fig. 3(b)). Indeed, a volume expansion was observed below $T \sim 40$ K in YbAgCu₄ [21], which is directly related to the sharp

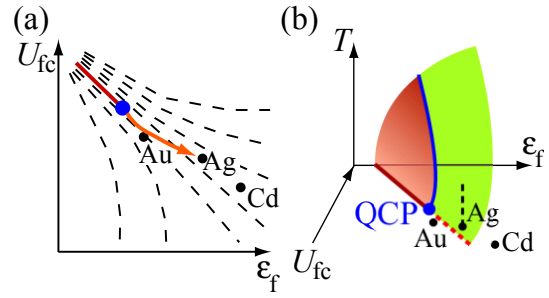


Figure 3 (color online) (a) Schematic contour plot of n_f , i.e., the Kondo temperature T_K in the ε_f - U_{fc} plane for the model (1) at $h = 0$. The FOVT line (solid line) terminates at the QCP (filled circle). The QCP reaches YbAgCu₄ by applying h about 40 T represented by an arrow. YbCdCu₄ is located far away from the QCP. The valence crossover surface reaches YbAuCu₄ by applying h about 1.3 T (see text). (b) Schematic T - ε_f - U_{fc} phase diagram at $h = 0$. YbAgCu₄ touches the valence-crossover surface at about $T = 40$ K. YbCdCu₄ is located too far from the QCP so that it needs too large T interval to reach the valence-crossover surface.

valence crossover from Yb^{+2.89} ($T > 40$ K) to Yb^{+2.87} ($T < 40$ K) [27].

3.2 YbAuCu₄ Recent ⁶³Cu NQR measurement in YbAuCu₄ has revealed that the characteristic temperature T_v^* emerges in the T - h phase diagram as illustrated in Fig. 4(a) [22]. Under the magnetic field for $h > 1$ T, as T decreases, ⁶³Cu NQR frequency ν_Q decreases sharply at $T_v^*(h)$. This indicates that the electric-field gradient at the Cu site changes sharply at $T_v^*(h)$, implying that the charge distribution changes drastically around the Cu site. This strongly suggests that the valence of Yb changes at $T_v^*(h)$. As h increases and across $h_v^* \sim 1.3$ T, the T^2 coefficient A of the resistivity sharply decreases, and the residual resistivity has a cusp-like peak structure at h_v^* [22]. These observations also suggest that the Yb-valence crossover temperature T_v^* is induced by applying the magnetic field.

This can be naturally understood if YbAuCu₄ is located just below the locus of the QCP as illustrated in Fig. 3(a). As shown in Fig. 2, for $h < T_K^{\text{QCP}}(h = 0)$, the valence-crossover line extends to the Kondo regime (dashed lines for $h = 0.02$ and 0.03 cross that for $h = 0$). Then, by applying h , the valence-crossover surface approaches and reaches the point indicated as Au in Fig. 3(a) at $h = 1.3$ T, which gives h_v^* in Fig. 4(a). As h further increases, the QCP moves as an arrow in Fig. 3(a). Hence, the valence-crossover temperature $T_v^*(h)$ increases as illustrated in Fig. 4(a). In the large h limit, the Yb³⁺ state is expected to be realized, since the Zeeman energy gain is mostly earned by the $n_f = 1$ state. Hence, $T_v^*(h)$ is expected to start to decrease for larger h , and finally to touch absolute zero. Indeed, this behaviour should appear if the valence QCP's exhibit the upturn as shown in Fig. 2.

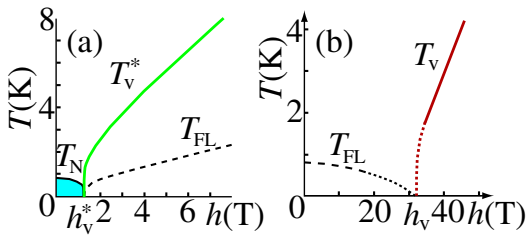


Figure 4 (color online) (a) T - h phase diagram of YbAuCu₄ [22]. The Neel temperature T_N is suppressed and the Yb valence crossover temperature T_v^* is induced for $h > h_v^* \sim 1.3$ T. (b) T - h phase diagram of CeIrIn₅ ($h \parallel c$) [33]. The first-order transition is induced for $h > h_v$ (solid line). In (a) and (b), For $T < T_{FL}$ (dashed line) the resistivity shows the Fermi liquid behaviour $\sim T^2$. In (b) dotted lines are guides for the eyes.

Here, we point out the close similarity of the T - h phase diagram between YbAuCu₄ [22] and YbRh₂Si₂ [28]. In YbRh₂Si₂, a very similar phase diagram as in Fig. 4(a) has been obtained with remarkable anomalies near $h \sim h_v$ such as the T -linear resistivity, residual resistivity peak, changes of the Hall coefficient, magnetostriction, and magnetization [28]. We stress here that these properties are explained if the system is close to the valence QCP, as mentioned above. Indeed, a band-structure calculation has shown that the change of the Hall coefficient around $h \sim h_v$ in YbRh₂Si₂ can be explained by a tiny Yb valence change [29]. Hence, it is important to examine the possibility experimentally whether the Yb valence changes at h_v in YbRh₂Si₂. Enhanced valence fluctuation is a possible origin of unconventional criticality observed in YbRh₂Si₂ [26].

3.3 CeIrIn₅ CeIrIn₅ is a heavy fermion metal, which exhibits the superconducting transition at $T \sim 0.4$ K. In the T - h phase diagram, the first-order-transition line emerges as illustrated in Fig. 4(b), which was detected by the jump in the magnetization curve [30-33]. Capan *et al.* observed anomalous behaviours that the residual resistivity increases as h approaches h_v . Furthermore, the power of the T dependence of resistivity shows a convex curve in the $T^{1.5}$ plot, which seems to indicate that the resistivity tends to show T -linear dependence. They pointed out that non-Fermi liquid behaviours even evident in $h = 0$ may be related to the metamagnetic anomaly at $h \sim h_v$, although its mechanism was not clarified [33].

Our results give a natural explanation for these anomalies: This is readily understood if CeIrIn₅ is located inside the enclosed area of the QCP line for $h \neq 0$ as in Fig. 2. Namely, at $h = 0$ the system is considered to be located at the valence-crossover regime (i.e., for $U < U_{fc}^{QCP}$ in Fig. 2, since no evidence of the first-order transition was observed in any physical quantities as a function of T at $h = 0$.) However, when h is applied, the QCP of

the FOVT approaches and eventually goes across, causing the metamagnetic transition in the magnetization curve. As mentioned above, near the QCP the residual resistivity is enhanced [15] and the T -linear resistivity is observed in the wide- T region [8], which are quite consistent with the observations [30-33]. Furthermore, the emergence of the first-order transition line in the T - h phase diagram is also in agreement with the present picture. We stress that CeCoIn₅ which has almost the same Fermi surfaces and similar crystalline-electric-field levels as those of CeIrIn₅ does not show such anomalies. This indicates that the viewpoint of the closeness to the valence QCP is also indispensable in understanding the Ce115 systems.

4 Summary We clarified the mechanism of how the QCP of the FOVT is controlled by the magnetic field. Even in the intermediate valence materials, the QCP of the FOVT is shown to be induced by applying the magnetic field. Valence fluctuations developed at the valence-crossover surface near the QCP cause various anomalies. We discussed that the proximity of the valence QCP resolves the outstanding puzzles observed in YbXCu₄ (X=Ag, Cd, Au) and CeIrIn₅. A key concept is the closeness to the QCP of the FOVT. Influence of the valence QCP offers a key origin in understanding unresolved anomalies in Ce- and Yb-based heavy fermions.

References

- [1] T. Moriya, Spin Fluctuations in Itinerant Electron Magnetism (Springer-Verlag, Berlin, 1985).
- [2] J. A. Hertz, Phys. Rev. B **14**, 1165 (1976).
- [3] A. J. Millis, Phys. Rev. B **48**, 7183 (1993).
- [4] K. Miyake, J. Phys.: Condens. Matter **19**, 125201 (2007).
- [5] K. A. Gschneidner and L. Eyring, Handbook on the Physics and Chemistry of Rare Earths (North-Holland, Amsterdam, 1978).
- [6] D. Wohlleben and J. Rohler, J. Appl. Phys. **55**, 15 (1984).
- [7] D. Jaccard, H. Wilhelm, K. Alami-Yadri, and E. Vargoz, Physica B **259-261**, 1 (1999).
- [8] A. T. Holmes, D. Jaccard, and K. Miyake, Phys. Rev. B **69**, 024508 (2004).
- [9] K. Fujiwara, Y. Hata, K. Kobayashi, K. Miyoshi, J. Takeuchi, Y. Shimaoka, H. Kotegawa, T. C. Kobayashi, C. Geibel, and F. Steglich, J. Phys. Soc. Jpn. **77**, 123711 (2008).
- [10] H. Q. Yuan, F. M. Grosche, M. Deppe, C. Geibel, G. Sparn, and F. Steglich, Science **302**, 2104 (2003).
- [11] H. Q. Yuan, F. M. Grosche, M. Deppe, C. Geibel, G. Sparn, C. Geibel, and F. Steglich, Phys. Rev. Lett. **96**, 047008 (2006).
- [12] K. Miyake, O. Narikiyo, and Y. Onishi, Physica B **259-261**, 676 (1999).
- [13] K. Miyake, T. Matsuura, and C. M. Varma, Solid State Commun. **71**, 1149 (1989).
- [14] T. M. Rice and K. Ueda, Phys. Rev. B **34**, 6420 (1986).
- [15] K. Miyake and H. Maebashi, J. Phys. Soc. Jpn. **71**, 1007 (2002).
- [16] Y. Onishi and K. Miyake, J. Phys. Soc. Jpn. **69**, 3955 (2000).

- [17] S. Watanabe, M. Imada, and K. Miyake, *J. Phys. Soc. Jpn.* **75**, 043710 (2006).
- [18] I. Felner and I. Nowik, *Phys. Rev. B* **33**, 617 (1986).
- [19] J. L. Sarrao, *Physica B* **259-261**, 128 (1999).
- [20] Y. H. Matsuda, T. Inami, K. Ohwada, Y. Murata, H. Nojiri, Y. Murakami, H. Ohta, W. Zhang, and K. Yoshimura, *J. Phys. Soc. Jpn.* **76**, 034702 (2007).
- [21] T. Koyama, M. Matsumoto, T. Tanaka, H. Ishida, T. Mito, S. Wada, and J. L. Sarrao, *Phys. Rev. B* **66**, 014420 (2002).
- [22] S. Wada, A. Yamamoto, K. Ishida, and J. L. Sarrao, *J. Phys.: Condens. Matter* **20**, 175201 (2008).
- [23] W. E. Pickett, A. J. Freeman, and D. D. Koelling, *Phys. Rev. B* **23**, 1266 (1981).
- [24] J. K. Freericks and V. Zlatic, *Phys. Rev. B* **58**, 322 (1998).
- [25] S. Watanabe, A. Tsuruta, K. Miyake, and J. Flouquet, *Phys. Rev. Lett.* **100**, 236401 (2008).
- [26] S. Watanabe and K. Miyake, *Phys. Rev. Lett.* **105**, 186403 (2010).
- [27] J. L. Sarrao, C. D. Immer, Z. Fisk, C. H. Booth, E. Figueroa, J. M. Lawrence, R. Modler, A. L. Cornelius, M. F. Hundley, G. H. Kwei, J. D. Thompson, and F. Bridges, *Phys. Rev. B* **59**, 6855 (1999).
- [28] P. Gegenwart, T. Westerkamp, C. Krellner, Y. Tokiwa, S. Paschen, C. Geibel, F. Steglich, E. Abrahams, and Q. Si, *Science* **315**, 969 (2007) and references therein.
- [29] M. R. Norman, *Phys. Rev. B* **71**, 220405R (2005).
- [30] T. Takeuchi, T. Inoue, K. Sugiyama, D. Aoki, Y. Tokiwa, Y. Haga, K. Kindo, and Y. Onuki, *J. Phys. Soc. Jpn.* **70**, 877 (2001).
- [31] J. S. Kim, J. Alwood, P. Kumar, and G. R. Stewart, *Phys. Rev. B* **65**, 174520 (2002).
- [32] E. C. Palm, T. P. Murphy, D. Halla, S. W. Tozera, R. G. Goodrich, and J. L. Sarrao, *Physica B* **329-333**, 587 (2003).
- [33] C. Capan, A. Bianchi, F. Ronning, A. Lacerda, J. D. Thompson, M. F. Hundley, P. G. Pagliuso, J. L. Sarrao, and R. Movshovich, *Phys. Rev. B* **70**, 180502 (2004).